

Direct Three-Dimensional Morphometric Analysis of Human Cancellous Bone: Microstructural Data from Spine, Femur, Iliac Crest, and Calcaneus

TOR HILDEBRAND,¹ ANDRES LAIB,¹ RALPH MÜLLER,² JAN DEQUEKER,³ and
PETER RÜEGSEGG¹

ABSTRACT

The appearance of cancellous bone architecture is different for various skeletal sites and various disease states. During aging and disease, plates are perforated and connecting rods are dissolved. There is a continuous shift from one structural type to the other. So traditional histomorphometric procedures, which are based on a fixed model type, will lead to questionable results. The introduction of three-dimensional (3D) measuring techniques in bone research makes it possible to capture the actual architecture of cancellous bone without assumptions of the structure type. This requires, however, new methods that make direct use of the 3D information. Within the framework of a BIOMED I project of the European Union, we analyzed a total of 260 human bone biopsies taken from five different skeletal sites (femoral head, vertebral bodies L2 and L4, iliac crest, and calcaneus) from 52 donors. The samples were measured three-dimensionally with a microcomputed tomography scanner and subsequently evaluated with both traditional indirect histomorphometric methods and newly developed direct ones. The results show significant differences between the methods and in their relation to the bone volume fraction. Based on the direct 3D analysis of human bone biopsies, it appears that samples with a lower bone mass are primarily characterized by a smaller plate-to-rod ratio, and to a lesser extent by thinner trabecular elements. (J Bone Miner Res 1999;14:1167–1174)

INTRODUCTION

BONE DISORDERS such as osteoporosis lead to alterations in cancellous bone. These alterations are not only characterized by a reduction of bone mass but also by structural changes in the microarchitecture of bone. Using a combination of bone density and architectural measures, the overall strength of trabecular bone is explained to 94%⁽¹⁾ compared with 64% if bone density is used alone.⁽²⁾ Information on the three-dimensional (3D) structure is therefore an important complement to measures of bone mineral density.

The standard procedure to examine structural properties of cancellous bone is based on 2D sections of bone biopsies.

Three-dimensional morphometric indices are derived from 2D images using stereological methods.⁽³⁾ Such techniques have been investigated extensively (e.g., Whitehouse⁽⁴⁾ and Parfitt et al.⁽⁵⁾). While indices such as relative bone volume (BV/TV) and surface density (BS/BV) are directly obtainable from 2D images, a range of important indices such as trabecular thickness (Tb.Th), trabecular separation (Tb.Sp), and trabecular number (Tb.N) are to be derived indirectly assuming a fixed structural model. Typically, ideal plate models or rod models are used. The assumption of a fixed model type, however, is critical since, due to aging and disease, trabecular bone might change its structure type continually. A deviation from the assumed model will lead to unpredictable errors in the indirectly derived indices.

¹Institute for Biomedical Engineering, University of Zürich and Swiss Federal Institute of Technology (ETH), Zürich, Switzerland.

²Orthopedic Biomechanics Laboratory, Harvard Medical School, Beth Israel Deaconess Medical Center, Boston, Massachusetts, U.S.A.

³Arthritis and Metabolic Bone Disease Research Unit, K.U. Leuven, University Hospital, Pellenberg, Belgium.

With the advent of 3D measuring techniques, it is now possible to explore the microarchitecture of cancellous bone directly without making assumptions on the structure type. Serial sectioning of embedded bone specimens⁽⁶⁾ allows the reconstruction of high-resolution 3D images. The method, however, entails substantial preparation of the samples, including embedding in black resin and surface treatment for contrast enhancement. Serial sectioning is furthermore inherently a destructive technique and does not allow subsequent analysis of the sample, e.g., mechanical testing or chemical analysis. Microcomputed tomography (MicroCT) is an alternative technique to image trabecular bone in three dimensions nondestructively and without tedious sample preparation. The first experimental system capable of producing 3D images had a spatial resolution of 50 μm using a microfocus X-ray tube.⁽⁷⁾ Now resolutions up to 2 μm can be achieved if synchrotron radiation is applied.⁽⁸⁾ In our study, we used the first commercially available MicroCT system. It is of the fan-beam type, operates with a microfocus X-ray tube and has a nominal resolution of 14 μm .⁽⁹⁾ Comparing the morphometric analysis of human bone biopsies performed with the MicroCT to conventional histologic sections, high correlations of the results obtained with the two procedures were found with $r > 0.84$.⁽¹⁰⁾

However, to make full use of the now available volumetric measuring techniques, new structure analysis procedures are required. Examples of such procedures are direct volume and surface determination,⁽¹¹⁾ model independent assessment of thickness,⁽¹²⁾ three-dimensional connectivity estimation,⁽¹³⁾ and 3D structure type assessment.⁽¹⁴⁾ An overview on 3D methods for the quantitation of cancellous bone architecture can be found in a recent review article.⁽¹⁵⁾

The purpose of this paper is to report on the results of 260 bone biopsies from five different skeletal sites of 52 subjects which were measured with 3D MicroCT and analyzed with standard histomorphometric procedures and with newly developed 3D procedures.

Materials

Trabecular bone samples were taken from 52 human cadavers (20 females, 32 males) with ages ranging from 24 to 92 years (mean 67.3, SD 15.5 years). For the purpose of the morphometric analysis, the samples were prepared in standardized conditions from the head of the right femur, the center of the second and fourth lumbar vertebral body, the calcaneus, and the anterior-superior part of the iliac crest. The subjects were selected from a total of 70 donors with the criterion of having all five samples from the mentioned sites per subject. A sample was excluded if it contained compact bone or if it could not be harvested in one connected piece or if it was missing due to prosthesis or amputations. Cause of death and medical history of the subjects were published in detail elsewhere,⁽¹⁶⁾ a short summary shall be given here only. In the framework of the European Union BIOMED I Concerted Action "Assessment of Bone Quality in Osteoporosis,"⁽¹⁷⁾ cadavers were collected consecutively over a period of 8 months (study protocol approved by the ethical committee of the Catholic

University of Leuven, Belgium). The bone cores were fixed after harvesting in phosphate buffered formaldehyde and stored at -20°C . The main causes of death were cardiogenic diseases, respiratory diseases, and cerebrovascular attacks. Medical archives were reviewed to obtain information on the fracture history, medications known to affect bone, and other pathologies. Nine percentage of the subjects had been under corticosteroids, and 20% had had diabetes mellitus.

MATERIALS AND METHODS

All samples were scanned with a high-resolution MicroCT system,⁽⁹⁾ which is commercially available under the name μCT 20 (Scanco Medical, Bassersdorf, Switzerland). The spatial resolution of the system is 28 μm , and cubic voxels with a side length of 14 μm were used to represent the measured object. The bone biopsies were placed in an airtight cylindrical sample holder filled with formaldehyde, and no further sample preparation was necessary for the microtomographic imaging. From the resulting voxel data, a cubic volume of interest with side length 4 mm was selected, corresponding to 286 voxels. The gray-value images were segmented using a low-pass filter to remove noise and a fixed threshold to extract the mineralized bone phase. From these images, the structural indices were assessed using both traditional indirect methods and newly developed direct techniques.

Primary indices

Bone surface area (BS) is calculated using the Marching Cubes method⁽¹⁸⁾ to triangulate the surface of the mineralized bone phase.⁽¹⁹⁾

Bone volume (BV) is calculated using tetrahedrons corresponding to the enclosed volume of the triangulated surface.⁽¹¹⁾

Total volume (TV) is the volume of the whole examined sample. To be able to compare samples with different sizes the normalized indices, BV/TV and BS/TV are used. The specific bone surface or bone surface-volume-ratio is given by BS/BV.

A more indirect way to calculate the primary indices would be to derive the involved surface area using methods such as mean intercept length (MIL) or 2D perimeter estimation. These methods were developed for the 2D analysis of trabecular bone but are also used for the analysis of 3D images.⁽²⁰⁾ A recent study shows that primary quantities derived in such a way may vary as much as 52% depending on which method is used.⁽²¹⁾

Traditionally derived indices

These indices are derived from the primary indices assuming a constant structure model (plate model) and applying stereological techniques.^(3,5,22)

Tb.Th is derived from the bone surface-to-volume ratio. For the plate model $\text{Tb.Th} = 2 \text{ BV/BS}$.

Tb.Sp can be interpreted as the thickness of the marrow

cavities and can consequently be derived from the marrow surface-to-volume ratio (MS/MV). For the plate model the relation is $Tb.Sp = 2 MV/MS = 2 (TV - BV)/BS$.

Tb.N is defined as the number of plates per unit length and can be calculated indirectly using the relation $Tb.N = 0.5 BS/TV$. Tb.N is thus equal to the inverse sum of Tb.Sp and Tb.Th.

Directly assessed indices

Three-dimensional images enable the direct assessment of metric indices by actually measuring distances in the 3D space. Such techniques do not rely on an assumed model type and are therefore not biased by eventual deviations of the actual structures from this model. The new, model-independent indices are marked with an asterisk.

Tb.Th* is determined by filling maximal spheres into the structure with the distance transformation.⁽¹²⁾ Then the average thickness of all bone voxels is calculated to give Tb.Th*

Tb.Sp* is calculated with the same procedure as used for the Tb.Th, but this time the voxels representing nonbone parts are filled with maximal spheres. The separation Tb.Sp* is thus the thickness of the marrow cavities.

Tb.N* is taken as the inverse of the mean distance between the midaxes of the observed structure. The midaxes of the structure are assessed from the binary 3D image using the 3D distance transformation and extracting the center points of nonredundant spheres which fill the structure completely. Then the mean distance between the midaxes is determined in analogy to the Tb.Sp* calculation, i.e., the separation between the midaxes is assessed.

Directly assessed nonmetric indices

The structure model index (SMI) is an estimation of the plate-rod characteristic of the structure.⁽¹⁴⁾ SMI is calculated by a differential analysis of a triangulated surface of a structure and is defined as

$$SMI = 6\{[BV(dBS/dr)]/BS^2\}$$

where dBS/dr is the surface area derivative with respect to a linear measure r , corresponding to the half thickness or the radius assumed constant over the entire structure. This derivative is estimated by a simulated thickening of the structure by translating the triangulated surface by a small extent in its normal direction and dividing the associated change of surface area with the length of the extent. For an ideal plate and rod structure the SMI value is 0 and 3, respectively. For a structure with both plates and rods of equal thickness, the value is between 0 and 3, depending on the volume ratio between rods to plates.

The geometrical degree of anisotropy (DA) is defined as the ratio between the maximal and the minimal radius of the MIL ellipsoid.⁽²³⁾ The MIL distribution is calculated by superimposing parallel test lines in different directions on the 3D image. The directional MIL is the total length of the test lines in one direction divided by the number of intersections with the bone-marrow interface of the test lines in

the same direction. The MIL ellipsoid is calculated by fitting the directional MIL to a directed ellipsoid using a least square fit.

RESULTS

Table 1 shows the basic descriptive statistics of the primary indices BV/TV, BS/TV, BS/BV, of the directly assessed indices Tb.Th*, Tb.Sp*, and Tb.N*, and of the traditionally derived indices Tb.Th, Tb.Sp, and Tb.N. The abbreviations used for the samples are the same as defined in the BIOMED I study: iliac crest (ICF), femoral head (FRA), second and fourth lumbar spine (LS2B and LS4A), and calcaneal core (CAB). Bone volume fraction ranges from 4% to 48% and bone surface density from 7 mm²/mm³ to 34 mm²/mm³. The largest bone volume fractions are found in the femoral head samples and the lowest ones in the lumbar spine samples. The samples from the calcaneal core and iliac crest have bone volume fractions in between and overlapping those found in the lumbar spine and femoral head. The interindividual scatter described by the coefficient of variation of the bone volume fraction is ~30% for each site, the one for bone surface density ~20%.

The directly measured trabecular thickness (Tb.Th*) ranges from 82 µm to 284 µm. The thickest trabeculae are found in the femoral head (194 ± 33 µm) followed by the iliac crest (151 ± 27 µm). In the lumbar spine and calcaneal core, the distributions of the Tb.Th are lower and similar (122–139 ± 18–28 µm). Compared with the directly assessed thickness, the indirectly calculated thickness (Tb.Th) is lower at all measured sites (21–43%). The best correspondence is observed in the femoral head and the poorest in the lumbar spine.

The directly calculated trabecular separation (Tb.Sp*) ranges from 0.45 mm to 1.31 mm. All sites have quite similar values. The indirectly calculated separations (Tb.Sp) are very different from the directly assessed ones (Fig. 1); the range is considerably larger (from 0.387 mm to 2.288 mm) and so is the scatter of the values at the individual sites with the exception of the data from the femoral head. It is interesting to note that the FRA samples are almost purely plate-like (see below).

The structure type of the samples as revealed by the SMI shows high interindividual variability at all examined sites and significant differences between the sites (Table 2). The structure of the femoral head is characterized by plates (ideal plates: SMI = 0), those of the lumbar spine by rods (ideal rods: SMI = 3). This can also be confirmed by visual inspection of the samples (Fig. 2). In the iliac crest and in the calcaneus, a more diverse structure type is found with both plate-like and rod-like samples (Fig. 3). The negative SMI values originate from the very dense samples (primarily femoral head) with a concave plate-like structure, sometimes referred to as a spherical void. The concave surface induces a negative value of the surface area derivative used in the calculation of SMI. The DA varies between 1.1 and 2.4 and is highest in the calcaneus and lowest in the lumbar spine. The differences between the examined sites, however, are small and not significant.

TABLE 1. DIRECT 3D MORPHOMETRIC INDICES OF 52 QUINTUPLES OF BONE SAMPLES: THE TRADITIONAL, INDIRECTLY DERIVED INDICES ARE GIVEN IN PARENTHESES

<i>Index</i>	<i>Site</i>	<i>Mean</i>	<i>SD</i>	<i>CV [%]</i>	<i>Median</i>	<i>Min</i>	<i>Max</i>
BV/TV (1)	ICF	0.156	0.054	34.8	0.151	0.048	0.279
	LS2B	0.083	0.024	28.6	0.083	0.040	0.158
	LS4A	0.087	0.033	37.8	0.082	0.040	0.226
	FRA	0.261	0.078	29.8	0.245	0.118	0.481
	CAB	0.120	0.035	29.3	0.120	0.054	0.190
BS/TV (mm ⁻¹)	ICF	2.54	0.64	25.0	2.65	0.99	3.94
	LS2B	1.87	0.49	26.3	1.82	1.01	2.95
	LS4A	1.71	0.45	26.1	1.66	0.84	2.85
	FRA	3.19	0.49	15.4	3.15	1.95	4.05
	CAB	2.05	0.46	22.3	2.09	1.10	2.93
BS/BV (mm ⁻¹)	ICF	17.65	3.45	19.6	17.60	10.84	32.13
	LS2B	23.73	3.41	14.4	23.40	17.16	34.29
	LS4A	21.17	3.59	17.0	20.95	11.37	32.94
	FRA	13.12	2.92	22.3	12.45	7.17	21.19
	CAB	21.64	3.23	14.9	22.05	14.50	28.34
Tb.Th* (mm) (Tb.Th)	ICF	0.151	0.027	18.1	0.148	0.087	0.225
		(0.117)	(0.023)	(19.5)	(0.113)	(0.062)	(0.184)
	LS2B	0.122	0.019	15.2	0.122	0.082	0.165
		(0.086)	(0.012)	(14.0)	(0.085)	(0.058)	(0.117)
	LS4A	0.139	0.028	20.0	0.134	0.092	0.224
		(0.097)	(0.018)	(18.9)	(0.094)	(0.061)	(0.176)
	FRA	0.194	0.033	17.1	0.193	0.127	0.284
		(0.160)	(0.035)	(21.9)	(0.154)	(0.094)	(0.279)
	CAB	0.129	0.018	13.7	0.124	0.102	0.169
		(0.095)	(0.015)	(16.1)	(0.090)	(0.071)	(0.138)
Tb.Sp* (mm) (Tb.Sp)	ICF	0.747	0.150	20.1	0.698	0.523	1.307
		(0.736)	(0.299)	(40.6)	(0.623)	(0.387)	(1.904)
	LS2B	0.792	0.135	17.0	0.759	0.572	1.268
		(1.067)	(0.327)	(30.7)	(0.988)	(0.607)	(1.889)
	LS4A	0.854	0.143	16.7	0.841	0.602	1.164
		(1.157)	(0.352)	(30.4)	(1.105)	(0.614)	(2.288)
	FRA	0.638	0.114	17.9	0.633	0.454	0.940
		(0.484)	(0.124)	(25.6)	(0.470)	(0.300)	(0.856)
	CAB	0.679	0.107	15.7	0.661	0.456	0.982
		(0.934)	(0.265)	(28.3)	(0.850)	(0.596)	(1.741)
Tb.N* (mm ⁻¹) (Tb.N)	ICF	1.402	0.265	18.9	1.421	0.788	2.051
		(1.272)	(0.318)	(25.0)	(1.327)	(0.496)	(1.970)
	LS2B	1.278	0.201	15.7	1.263	0.770	1.774
		(0.933)	(0.245)	(26.3)	(0.913)	(0.503)	(1.474)
	LS4A	1.161	0.181	15.5	1.144	0.843	1.609
		(0.855)	(0.223)	(26.1)	(0.834)	(0.420)	(1.423)
	FRA	1.595	0.292	18.3	1.497	1.092	2.387
		(1.593)	(0.246)	(15.4)	(1.579)	(0.974)	(2.024)
	CAB	1.462	0.202	13.7	1.455	0.998	2.090
		(1.027)	(0.229)	(22.3)	(1.046)	(0.551)	(1.465)

To see which indices might have a potential of giving structural information beyond bone mass, linear and logarithmic regression were performed with the bone volume fraction as the independent variable (Table 3). This also reveals differences between direct and indirect methods for the assessment of structural indices. Most remarkable are the relatively low correlations for Tb.Th* and Tb.Sp* if direct, model-independent methods are used. This is in contrast to the quite high correlations found with model-dependent procedures. To stress this point, Fig. 4 is given.

SMI shows a strong negative correlation with BV/TV. An interesting fact is that the same trend is found for each site separately, fitting almost the same regression line. The

correlations are a bit lower, especially in the lumbar spine ($r^2 = 0.33$ – 0.40 , $p < 0.001$).

DISCUSSION

In this paper, a total of 260 human bone biopsies taken at five different skeletal sites from 52 donors were measured using a MicroCT system and analyzed with newly developed 3D methods and standard histomorphometric procedures.

The results show large intersite and intrasite differences. In the femoral head, high bone volume fractions are ob-

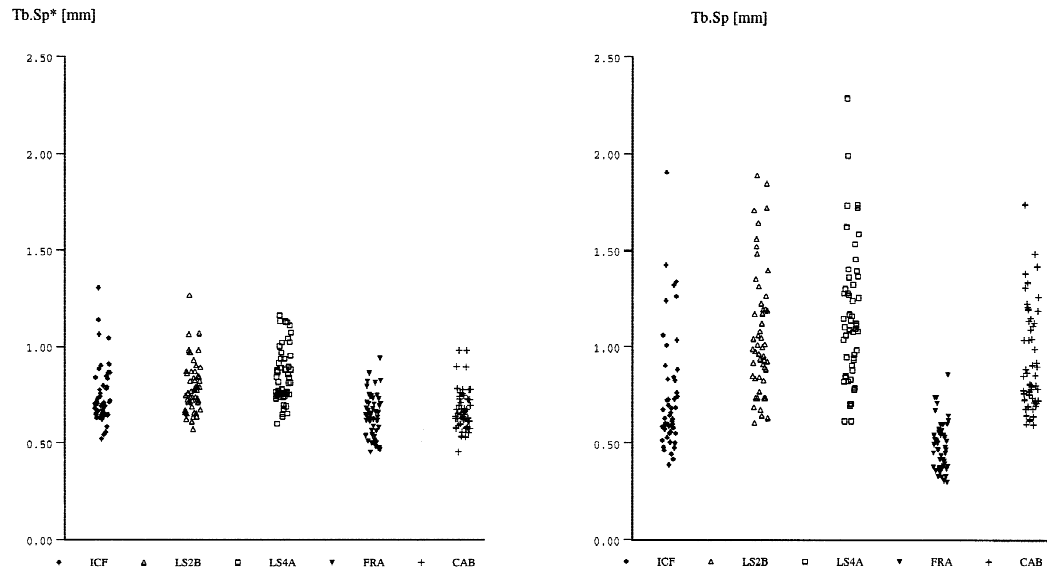


FIG. 1. Distribution of direct and indirect separation Tb.Sp* and Tb.Sp at all examined skeletal sites.

TABLE 2. NONMETRIC 3D INDICES OF 52 QUINTUPLES OF BONE SAMPLES

Index	Site	Mean	SD	CV [%]	Median	Min	Max
SMI (1)	ICF	1.15	0.61	53.3	1.05	-0.70	2.53
	LS2B	2.13	0.35	16.6	2.18	1.24	2.88
	LS4A	2.12	0.36	17.3	2.15	0.64	2.74
	FRA	0.41	0.68	16.3	0.47	-2.57	1.74
	CAB	1.76	0.36	20.7	1.76	1.03	2.36
DA [1]	ICF	1.49	0.18	12.0	1.45	1.24	1.97
	LS2B	1.42	0.16	11.6	1.41	1.15	1.96
	LS4A	1.51	0.16	11.0	1.50	1.13	1.95
	FRA	1.68	0.18	10.8	1.68	1.29	2.38
	CAB	1.75	0.15	8.5	1.72	1.44	2.17

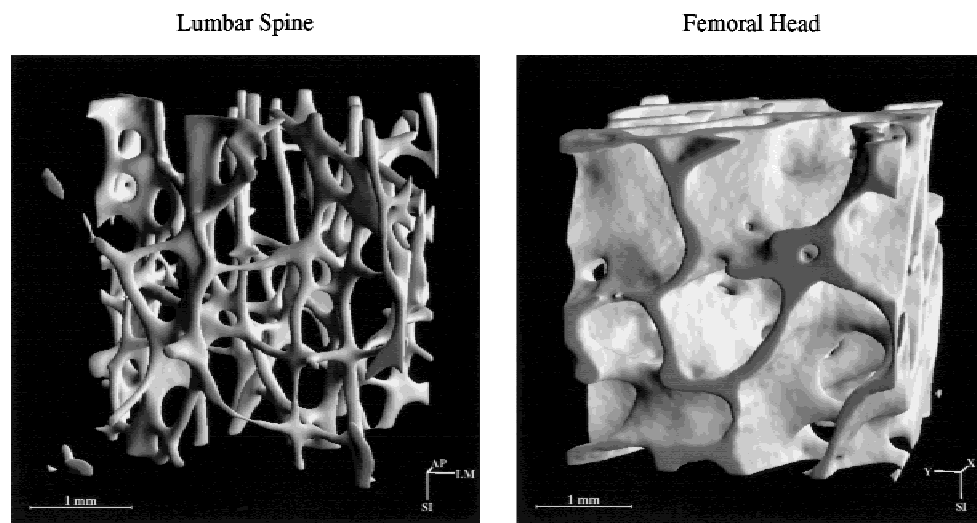


FIG. 2. Typical cancellous bone structures of the lumbar spine and the femoral head. In the lumbar spine rod-like trabeculae dominate (left, SMI = 2.5). The trabecular structure found in femoral head, however, is in general more plate-like (right, SMI = 0.16).

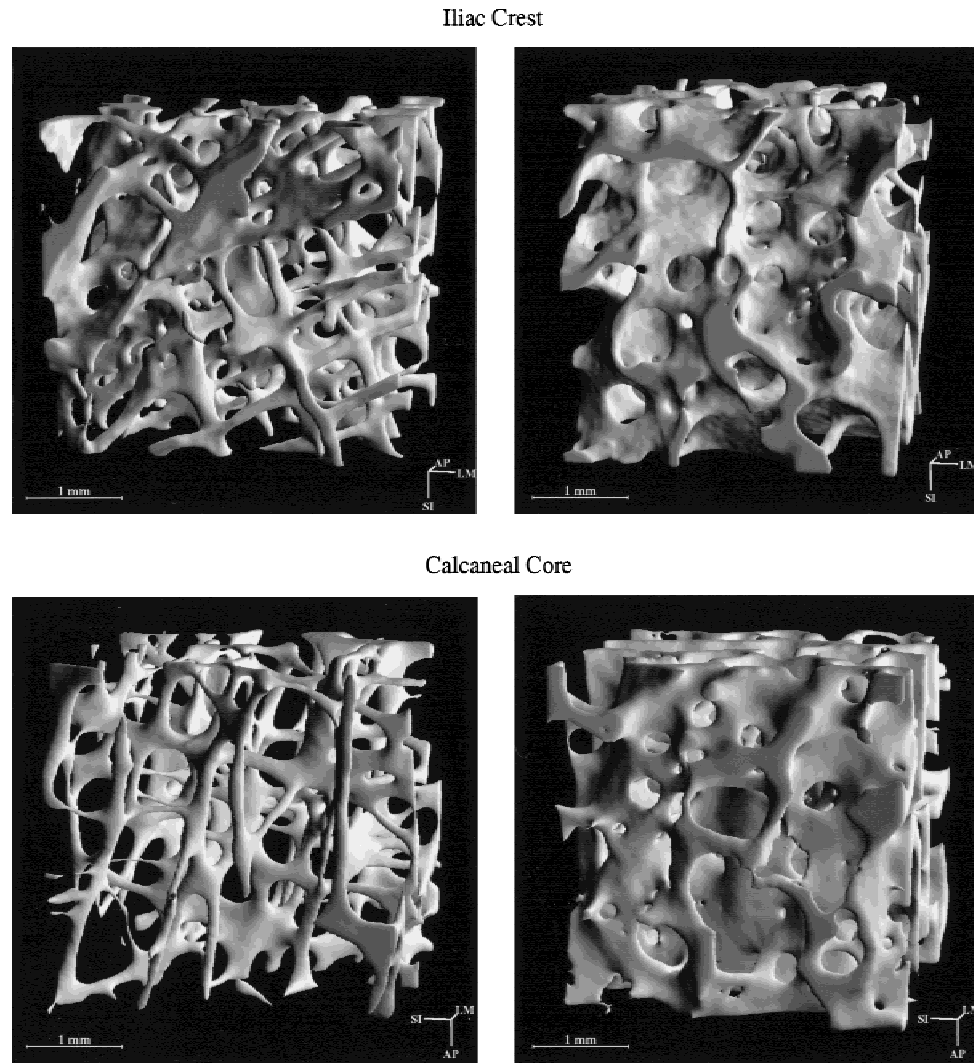


FIG. 3. In the samples of iliac crest and the calcaneus the structure cannot be associated with a single model. In the iliac crest, both rod-like (top left, SMI = 2.1) and plate-like (top right, SMI = 0.8) samples can be observed. In the calcaneus, most examined samples were rod-like (bottom left, SMI = 2.3), but several samples with plate-like structure were also found (bottom right, SMI = 1.1).

TABLE 3. CORRELATION COEFFICIENTS R^2 BETWEEN STRUCTURAL INDICES AND BONE VOLUME FRACTION

r^2 with BV/TV	Iliac crest	2nd lumbar spine	4th lumbar spine	Femoral head	Calcaneal core
Tb.N*	0.743 [†]	0.399 [†]	0.338 [†]	0.708 [†]	0.353 [†]
Tb.N	0.710 [†]	0.734 [†]	0.675 [†]	0.514 [†]	0.789 [†]
Tb.Th*	0.330 [†]	0.075	0.427 [†]	0.633 [†]	0.359 [†]
Tb.Th	0.573 [†]	0.189 [‡]	0.581 [†]	0.753 [†]	0.544 [†]
Tb.Sp*	0.467 [†]	0.368 [†]	0.411 [†]	0.479 [†]	0.368 [†]
Tb.Sp	0.663 [†]	0.737 [†]	0.627 [†]	0.735 [†]	0.785 [†]
SMI	0.723 [†]	0.334 [†]	0.397 [†]	0.796 [†]	0.644 [†]
DA	0.134 [‡]	0.154 [‡]	0.242 [†]	0.164 [‡]	0.052

[†] $p < 0.001$; [‡] $p < 0.01$.

served, trabeculae are thick, and the structure is typically plate-like. In the lumbar spine, bone volume is low, trabeculae are thin, and the structure is rod-like. In the calcaneus, the structure is similar to the one found in the lumbar spine

but with a slightly higher bone volume fraction. The indices derived from the iliac crest are distributed between and overlap those found for the other sites which might suggest that the trabecular structure of the iliac crest is a mixture of

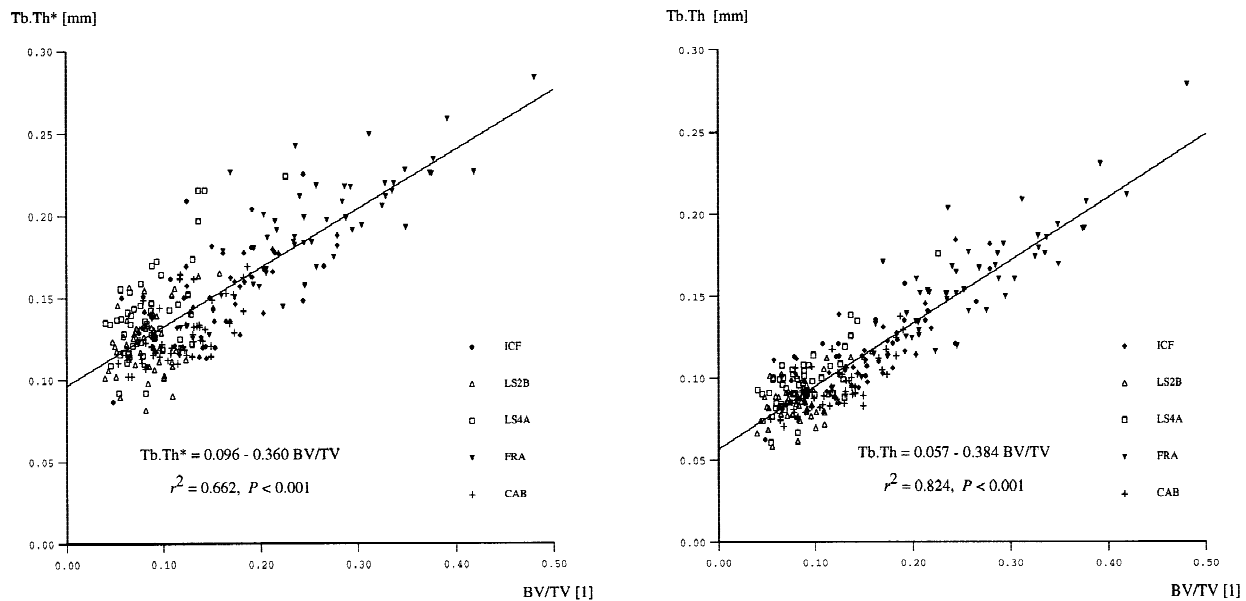


FIG. 4. Correlation between trabecular thickness (model-independent Tb.Th* on the left, model-dependent Tb.Th on the right) and bone volume density (BV/TV) for the samples of all analyzed sites.

the type of structure found in the femoral head and the lumbar spine. The distribution of the SMI values, however, shows a separation of the structure type among the samples rather than a mixed structure type: about one third of the samples have SMI values similar to those of the lumbar spine samples (rod-like) and the rest are close to the SMI values of the femoral head (plate-like).

The model-independent Tb.Th* is systematically higher than Tb.Th assessed with the plate-model assumption. The reason for this is seen in the deviation of the trabecular structure from the ideal plate model. There are always rods present, which cause the surface-to-volume ratio to be higher at a given thickness with the consequence of a smaller apparent thickness derived from BV/BS. Even in the femoral head, with its pronounced plate-like structure, the thickness is underestimated on average by 17%. As expected, the largest underestimation is observed in the lumbar spine (30%) due to the rod-like structure at this site. One would expect that assuming a rod model would be more adequate to derive thicknesses at the lumbar spine. If the rod model is used, however, thickness is overestimated on average by 41%. The correlation coefficient of Tb.Th versus BV/TV is considerably higher than Tb.Th* versus BV/TV. This can be explained by the definition of Tb.Th, which contains also BV, so Tb.Th is per se dependent on BV/TV, whereas the determination of Tb.Th* is really independent from that of BV/TV. We think, therefore, that the larger scatter of the data seen for the directly determined thickness is closer to reality. It might be noted here that similar observations were made in two dimensions, when directly and indirectly calculated trabecular widths were compared⁽²⁴⁾; the indirectly derived widths increasingly underestimated the directly measured ones as the relative bone area decreased. The weaker correlation found in our work for the directly determined thickness corre-

sponds also to the observation that bone loss is not primarily the result of trabecular thinning.⁽⁵⁾ In view of the strong correlation between SMI and BV/TV, found individually for every site, it appears that samples with a lower bone mass are primarily characterized by a smaller plate-to-rod ratio, and to a lesser extent by thinner trabecular elements.

Another issue of great interest is how structural indices relate to mechanical properties of bone. Such information could be used to derive the mechanical quality of bone from available structural indices. The introduction of large scale finite element (FE) analysis⁽²⁵⁾ and the availability of sufficient computer power make it possible to treat very large models of trabecular bone, e.g., to solve the corresponding FE models of the 3D images used in this study containing over one million elements.⁽²⁶⁾ These FE computations provide mechanical indices in a direct 3D way. Relations between mechanical and structural indices are valuable since they can explain which structural features are important for the mechanical stability of bone. This information might also be important for an early identification of bone disorders: structural changes might occur at an early stage even before the mechanical properties reach a critical level. Recent studies show that some structural indices are even available in vivo in time-serial examinations, although with a lower resolution in humans.⁽²⁷⁾

With the advent of high resolution 3D measurements, a new way to look at trabecular bone architecture becomes available. To make full use of the spatial information, however, it is necessary also to adapt the evaluation procedures.

Further studies, and especially a transfer of the 3D procedures to in vivo examinations, will show if a combination of structure and density indices leads to a better understanding of bone quality.

ACKNOWLEDGMENTS

This work was supported in part by grant 31-29971.90 from the Swiss National Science Foundation and by European Union Concerted Action BIOMED I: "Assessment of Quality of Bone in Osteoporosis," no. BMH1-CT92-0296. This article also serves as an official report of this study regarding the findings from the structural analysis based on MicroCT.

REFERENCES

1. Turner CH, Rho JY, Ashman RB, Cowin SC 1988 The dependence of elastic constants of cancellous bone upon structural density and fabric. *Trans Orthopaed Res Soc* **13**:74.
2. Rice JC, Cowin SC, Bowman JA 1988 On the dependence of elasticity and strength of cancellous bone on apparent density. *J Biomech* **22**:155-168.
3. Weibel ER 1980 *Stereological Methods*, Vol. 2: Theoretical Foundations. Academic Press, London, U.K.
4. Whitehouse WJ 1974 The quantitative morphology of anisotropic trabecular bone. *J Microsc* **101**:153-168.
5. Parfitt AM, Mathews CHE, Villanueva AR, Kleerekoper M, Frame B, Rao DS 1983 Relationships between surface, volume, and thickness of iliac trabecular bone in aging and in osteoporosis. *Calcif Tissue Int* **72**:1396-1409.
6. Odgaard A, Andersen K, Melsen F, Gundersen HJG 1990 A direct method for fast three-dimensional serial reconstruction. *J Microsc* **159**:335-342.
7. Feldkamp LA, Goldstein SA, Parfitt AM, Jesion G, Kleerekoper M 1989 The direct examination of three-dimensional bone architecture in vitro by computed tomography. *J Bone Miner Res* **4**:3-11.
8. Bonse U, Busch F, Günnewig O, Beckmann F, Pahl R, Delling G, Hahn M, Graeff W 1994 3D computed X-ray tomography of human cancellous bone at 8 μm spatial and 10-4 energy resolution. *Bone Miner* **25**:25-38.
9. Rügsegger P, Koller B, Müller R 1996 A microtomographic system for the non-destructive evaluation of bone architecture. *Calcif Tissue Int* **58**:24-29.
10. Müller R, Van Campenhout H, Van Damme B, Van Der Perre G, Dequeker J, Hildebrand T, Rügsegger P 1998 Morphometric analysis of human bone biopsies: A quantitative structural comparison of histological sections and micro-computed tomography. *Bone* **23**:59-66.
11. Guilak F 1994 Volume and surface area of viable chondrocytes in situ using geometric modelling of serial confocal sections. *J Microsc* **173**:245-256.
12. Hildebrand T, Rügsegger P 1997 A new method for the model independent assessment of thickness in three-dimensional images. *J Microsc* **185**:67-75.
13. Odgaard A, Gundersen HJG 1993 Quantification of connectivity in cancellous bone, with special emphasis on 3-D reconstructions. *Bone* **14**:173-182.
14. Hildebrand T, Rügsegger P 1997 Quantification of bone microarchitecture with the structure model index. *Comp Meth Biomech Biomed Eng* **1**:15-23.
15. Odgaard A 1997 Three-dimensional methods for quantification of cancellous bone architecture. *Bone* **20**:315-328.
16. Aerssens J, Boonen S, Joly J, Dequeker J 1997 Variations in trabecular bone composition with anatomical site and age: Potential implication for bone quality assessment. *J Endocrinol* **155**:411-421.
17. Dequeker J 1994 Assessment of quality of bone in osteoporosis BIOMED I: Fundamental study of relevant bone. *Clin Rheumatol* **13** (Suppl 1):7-12.
18. Lorensen WE, Cline HE 1987 Marching Cubes: A high resolution 3D surface construction algorithm. *Computer Graphics* **21**:163-169.
19. Müller R, Hildebrand T, Rügsegger P 1994 Non-invasive bone biopsy: A new method to analyse and display the three-dimensional structure of trabecular bone. *Phys Med Biol* **39**:145-164.
20. Goulet RW, Goldstein SA, Ciarelli MJ, Kuhn JL, Brown MB, Feldkamp LA 1994 The relationship between the structural and orthogonal compressive properties of trabecular bone. *J Biomech* **27**:375-389.
21. Simmons GA, Hipp JA 1997 Method-based differences in the automated analysis of three-dimensional morphology of trabecular bone. *J Bone Miner Res* **12**:942-947.
22. Parfitt AM, Drezner MK, Glorieux MK, Kanis FH, Malluche JA, Meunier PJ, Ott SM, Recker RR 1987 Bone histomorphometry: Standardization of nomenclature, symbols and units. Report of the ASBMR histomorphometry nomenclature committee. *J Bone Miner Res* **21**:595-610.
23. Harrigan TP, Mann RW 1984 Characterization of microstructural anisotropy in orthotropic materials using a second rank tensor. *J Mater Sci* **19**:761-767.
24. Birkenhäger-Frenkel DH, Couprou P, Hüpscher EA, Clermonts E, Coutinho MF, Schmitz PIM, Meunier PJ 1988 Age-related changes in cancellous bone structure, a two-dimensional study in the transiliac iliac crest biopsy sites. *Bone Miner* **4**:197-216.
25. Van Rietbergen B, Weinans H, Huiskes R, Odgaard A 1995 A new method to determine trabecular bone elastic properties and loading using micromechanical finite-element models. *J Biomech* **28**:69-81.
26. Ulrich D, Hildebrand T, Van Rietbergen B, Müller R, Rügsegger P 1997 The quality of trabecular bone evaluated with micro-computed tomography, FE-A and mechanical testing. In: Lowet G, Rügsegger P, Weinans H, Meunier A (eds.) *Bone Research Biomechanics*. IOS Press, Amsterdam, the Netherlands, pp. 97-112.
27. Laib A, Hildebrand T, Häuselmann HJ, Rügsegger P 1997 Ridge number density: A new parameter for in vivo bone structure analysis. *Bone* **21**:541-546.

Address reprint requests to:

Peter Rügsegger
Institute of Biomedical Engineering
ETH and University Zürich
Moussonstrasse 18
CH-8044 Zürich, Switzerland

Received in original form June 11, 1998; in revised form November 10, 1998; accepted December 30, 1998.